THE JOURNAL OF BIOLOGICAL CHEMISTRY VOL. 291, NO. 36, pp. 18856–18866, September 2, 2016
© 2016 by The American Society for Biochemistry and Molecular Biology, Inc. Published in the U.S.A.

Increased Activity of Src Homology 2 Domain Containing Phosphotyrosine Phosphatase 2 (Shp2) Regulates Activity-dependent AMPA Receptor Trafficking*

Received for publication, January 7, 2016, and in revised form, June 29, 2016 Published, JBC Papers in Press, July 14, 2016, DOI 10.1074/jbc.M116.714501

Bin Zhang, Yong-lan Du, Wen Lu, Xun-yi Yan, Qian Yang, Wei Yang, and Jian-hong Luo[1]

From the Department of Neurobiology, Key Laboratory of Medical Neurobiology (Ministry of Health of China), Collaborative Innovation Center for Brain Science, Zhejiang University School of Medicine, Hangzhou, Zhejiang 310058, China

Long term synaptic plasticity, such as long term potentiation (LTP), has been widely accepted as a cellular mechanism underlying memory. Recently, it has been unraveled that Shp2 plays a role in synaptic plasticity and memory in *Drosophila* and mice, revealing significant and conserved effects of Shp2 in cognitive function. However, the exact mechanism underlying this function of Shp2 in synaptic plasticity and memory still remains elusive. Here, we examine the regulation of Shp2 in hippocampal LTP and contextual fear conditioning. We find that Shp2 is rapidly recruited into spines after LTP induction. Furthermore, the phosphorylation level of Shp2 at Tyr-542 is elevated after LTP stimuli either in cultured hippocampal neurons or acute slices. Notably, contextual fear conditioning also regulates the phosphorylation level of Shp2 at Tyr-542, suggesting fine-tuned regulation of Shp2 in LTP and memory formation. By using a Shp2-specific inhibitor and adeno-associated virus-Cre mediated Shp2 knock-out in cultured neurons, we provide evidence that the phosphatase activity of Shp2 is critical for activity-dependent AMPA receptor surface trafficking. Collectively, our results have revealed a regulatory mechanism of Shp2 underlying LTP and memory, broadening our understanding of Shp2 in cognitive function.

Shp2, encoded by the gene *PTPN11*, is a ubiquitously expressed phosphatase possessing a structure containing two tandem SH2[2] (Src homology 2) domains flanked on its N terminus, followed by a protein-tyrosine phosphatase domain and a C-terminal hydrophilic tail containing phosphorylation sites (1, 2). The distinctive structural feature of Shp2 confers it playing two functional roles in signaling transduction. One function of Shp2 is conducting as an adaptor protein to assemble the multiple protein complex by its SH2 domain associating other phosphorylated tyrosine-containing proteins (2), the other is acting as a phosphatase to dephosphorylate its substrate upon certain stimuli. Tyrosine 542 of Shp2 at its hydrophilic tail is identified as a major phosphorylation site in response to growth factor stimuli (3). Previous studies argued that phosphorylation of Tyr-542 correlated with its phosphatase activity and promoted the activity of Shp2 by relieving the basal inhibition of protein-tyrosine phosphatase via disruption of intramolecular interaction of its tail with its N-SH2 domain (1, 3–5).

Long term synaptic plasticity, *i.e.* long term potentiation (LTP), and its opposing effect, long term depression are widely accepted as a cellular mechanism of memory (6). At glutamatergic synapses, LTP is expressed by a synapse-specific increase in the number of AMPA receptors at postsynaptic sites (7). In recent years, several studies unveiled the significance of Shp2 in cognitive function and long term memory. Genetic manipulation, *e.g.* knock-in mice with Noonan syndrome (NS) mutation of Shp2, and ablation of Shp2, no matter in *Drosophila* or rodents, both reveal that Shp2 is profoundly involved in synaptic plasticity and memory (8–10). However, genetic approaches *in vivo* can hardly avoid some unpredicted defects as well as side effects that were exemplified by excess weight displayed in the Shp2 knock-out (KO) mice (8) and other similar NS patient defects associated with NS mouse models derived from the knock-in Shp2 mutation (9). Although previous studies provide convincing evidences that proper Shp2 function is requisite of normal cognitive function and memory, the exact mechanism of Shp2 underlying synaptic plasticity and memory yet remains to be resolved in detail. Besides, the regulation of Shp2 in response to synaptic plasticity, such as its phosphatase activity, which is represented by the phosphorylation level of Tyr-542, has thus far been unknown. Importantly, advancement of understanding in regulation of Shp2 activity in synaptic plasticity and memory should throw light on the development of therapeutic approaches to mental diseases associated with dysfunctional Shp2. Therefore, we determined to examine the regulation of Shp2 in synaptic plasticity, especially in LTP.

In the present study, we investigated the regulation of Shp2 activity in synaptic plasticity. We found up-regulation of Shp2 phosphatase activity during LTP. Furthermore, we demonstrated that Shp2 was required for synaptic delivery of AMPA receptors using both pharmacological and genetic procedures. Combined with previous studies on loss of function of Shp2, we suggest that the activity of Shp2 is delicately regulated in synaptic plasticity. Additionally, at least to some extent, the phos-

* This work was supported by Natural Science Foundation of China Grants 91232303, 81221003, and 81561168022, National Basic Research Program of China Grant 2014CB910300, and the Fundamental Research Funds for the Central Universities of China. The authors declare that they have no conflict of interest with the contents of this article.

[1] To whom correspondence should be addressed: 866 Yu-hang-tang Rd., Hangzhou, Zhejiang 310058, China. Fax: 86-571-88981230; E-mail: luojianhong@zju.edu.cn.

[2] The abbreviations used are: SH2, Src homology domain 2; LTP, long term potentiation; STORM, stochastic optical reconstruction microscopy; AAV, adeno-associated virus; HFS, high-frequency stimulation; ANOVA, analysis of variance; TBST, Tween 20, Tris-buffered saline; DIV, days *in vitro*; PSD, postsynaptic density; cLTP, chemical LTP.

phatase activity of Shp2 is required for AMPA receptor delivery in LTP.

Results

Expression Profile of Shp2 and Phosphorylated Shp2 at Tyr-542 in Brain—Shp2 is highly expressed in the rat brain and widely distributed throughout numerous brain regions (11). Distinct phosphorylation levels of Tyr-542, which exists in several brain regions may imply a region-specific function. So we first set out to examine the status of phosphorylated Shp2 at Tyr-542 (named Tyr(P)-542) *in vivo*. Medial prefrontal cortex, hippocampus, thalamus, cerebellum, amygdala, pons, and striatum of adult mouse brain were collected and homogenized to analyze the expression level of Tyr(P)-542 in these brain regions. We found that total Shp2 was uniformly expressed throughout the brain with a phosphorylation level of Tyr-542 (evaluated as a ratio to total Shp2) exhibiting relatively much higher in the pons (Fig. 1, *A* and *B*). To ensure the accuracy of regions isolated in our experiments, the expression pattern of GluN2B was also assessed. As expected, it was in line with a previous study (Fig. 1, *A* and *B*) (12).

Shp2 was reported to exist in the synaptic plasma membrane (11), so we determined to explore the subcellular location of Shp2 and p-Shp2 at Tyr-542 with a successfully separated membrane fraction (P2), a Triton-insoluble postsynaptic density (also considered as PSD) fraction, and a non-PSD fraction of hippocampus. We found that Shp2 was enriched in the non-PSD fraction, whereas the Tyr(P)-542 level exhibited relatively much higher in the PSD fraction (Fig. 1, *C* and *D*). Moreover, a confocal image revealed that Shp2 (0.70 ± 0.012, $n = 36$) and p-Shp2 at Tyr-542 (0.67 ± 0.0089, $n = 36$) was robustly colocalized with PSD95, a scaffolding protein as a postsynaptic marker, in cultured hippocampal neurons (Fig. 1, *E* and *F*). Three-dimensional rendering of Shp2 and p-Shp2 at Tyr-542 colocalized with PSD95 with Z-stack images deprived from confocal microscopy demonstrated that both Shp2 and Tyr(P)-542 were localized adjacent to postsynaptic sites (Fig. 1*G*). To further confirm this result, a super-resolution image technology called stochastic optical reconstruction microscopy (STORM) was employed and subsequently we found Shp2 partially colocalized with PSD95 in dendrites (Fig. 1*H*). This unique positioning of Shp2 and p-Shp2 at Tyr-542 suggests that Shp2 was situated at the postsynaptic site and possibly plays a crucial role in the synaptic signaling transduction in dendritic spines.

Gain of function of Shp2 has been implicated in relationship to Noonan syndrome, which is a systemic developmental disorder (13). Thus, we sought to examine the developmental profile of Shp2 and p-Shp2 at Tyr-542 (3, 5). We evaluated the expression of GluN2A, Shp2, and p-Shp2 at the Tyr-542 level during development by immunoblotting extracts of hippocampus from mice at different ages. As a previous study showing a substantial increase of GluN2A expression level during development (14), our development profile of GluN2A was in accordance with that study. Remarkably, we found that the Tyr(P)-542 level was elevated with the total expression level of Shp2 being reduced during development (Fig. 1, *I* and *J*). The differences in expression levels between Shp2 and Tyr(P)-542 during development suggest the activity of Shp2 is finely tuned in neuron development.

Recruitment of Shp2 into Postsynaptic Density during LTP Induction—Proper function of Shp2 has been shown to be dispensable for normal LTP and memory (8–10). Both theoretical and experimental work suggests that the movement of molecules and organelles between the spine and the adjacent dendritic shaft contributes to synaptic activity (15). Therefore, examining the translocation of Shp2 in different subcellular fractions during the activity may reveal its functional role. We analyzed the translocation of endogenous Shp2 and GluA1 by subcellular fractionation of the CA1 region of a hippocampal slice after high-frequency (100 Hz/1 s) stimulation (HFS). The field EPSP during the last 5 min of recording clearly demonstrated that HFS elicited a substantial increase in slope of EPSP. We then determined that Shp2 was significantly increased in the PSD fraction after LTP induction at 10 min (2.91 ± 0.34, $p < 0.005$, two-tailed Student's *t* test, $n = 4$) without change in the P2 fraction (1.10 ± 0.14, $n = 4$) (Fig. 2, *B* and *C*). We also observed accumulation of GluA1 of the AMPA receptor (1.76 ± 0.16, $p < 0.01$, two-tailed Student's *t* test, $n = 4$) in the PSD fraction after LTP induction, which was consistent with our previous report (16).

To reinforce this conclusion, we investigated colocalization between Shp2 and PSD95 in dendrites with and without cLTP stimuli using a standard protocol (17, 18) that selectively activates synaptic NMDA receptors. Statistical analysis of the colocalization illustrated that the proportion of Shp2 clusters (without cLTP treatment, 0.69 ± 0.0056, $n = 15$ neurons; cLTP treatment, 0.73 ± 0.0054, $n = 15$ neurons; two-tailed Student's *t* test, $p < 0.005$) that were merged with PSD95 clusters was markedly increased in the cLTP group (Fig. 2, *D* and *E*). The results from biochemistry and confocal images mentioned above suggest increased incorporation of Shp2 into excitatory postsynaptic sites after LTP induction.

The Activity of Shp2 Is Up-regulated during LTP Stimulation and Contextual Fear Conditioning—Given enrichment of Shp2 in the postsynaptic fraction after LTP induction, we postulated that the activity of Shp2 was strictly regulated and thus it played an important role in synaptic activity. Therefore, we treated cultured hippocampal neurons with bicuculline, which is an antagonist of GABA receptor to increase basal excitatory synaptic activity of neurons. In our experiment, short term exposure to bicuculline (25 μM; 5–15 min) elevated the Tyr(P)-542 level (5 min treatment, 2.71 ± 0.37, $p < 0.01$; 10 min treatment, 3.27 ± 0.27, $p < 0.005$; 15 min treatment, 2.90 ± 0.49, $p < 0.01$, *versus* Ctl, one-way ANOVA, $n = 6$) in neurons without affecting the total Shp2 level, indicating that the Tyr-542 level of Shp2 can be regulated rather quickly by neuronal activity (Fig. 3, *A* and *B*).

To further explore the regulation of Shp2 in synaptic activity, we examined the phosphorylation level of Shp2 at Tyr-542 after HFS in a acute slice preparation. We found increased average responses during the last 5 min of the recording indicating a successful LTP (Fig. 2*C*). We collected CA1 mini slices from male mice (5–6 weeks) after HFS, the lysate was subjected to immunoblot analysis. As shown in Fig. 3, *D* and *E*, phosphorylation of GluA1 Ser-845 was elevated during the acute phase (10

min, 2.43 ± 0.11, $p < 0.005$, LTP *versus* Ctl, one-way ANOVA, $n = 4$) and maintain phase (60 min, 2.16 ± 0.14, $p < 0.005$, LTP *versus* Ctl, one-way ANOVA, $n = 4$), indicating a successful LTP induction. Likewise, the Tyr(P)-542 level was substantially increased at both time points (10 min, 1.96 ± 0.19, $p < 0.05$; 60 min 2.25 ± 0.31, $p < 0.01$, LTP *versus* Ctl, one-way ANOVA,

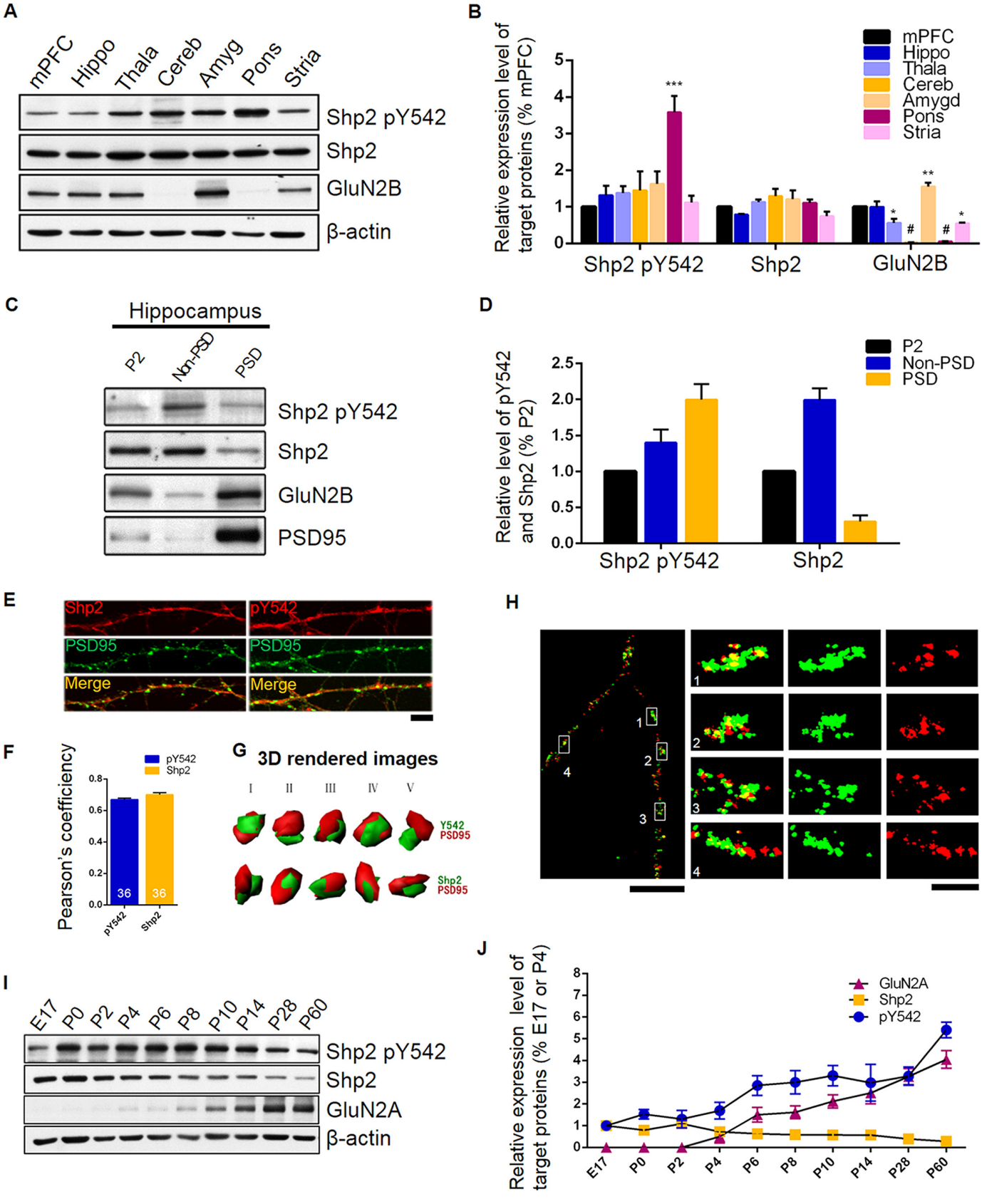

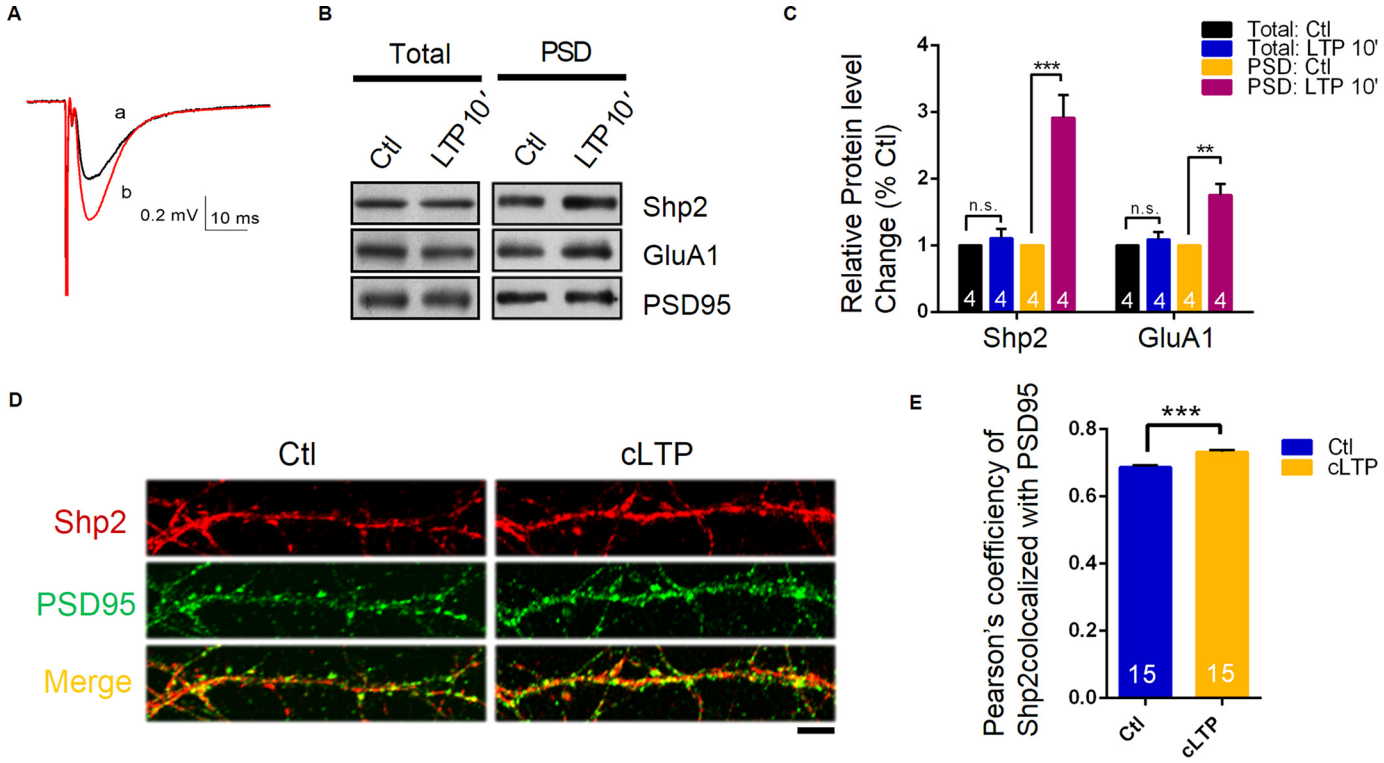

FIGURE 2. **Shp2 is recruited into the postsynaptic site after LTP induction.** *A*, sample traces show average responses during baseline (*black*) and the last 5 min (*red*) of the recording. *Scale bar*, 0.2 mV/10 ms. *B*, Western blot analysis of total and PSD fractions from control or LTP induced slices ($n = 4$). *C*, summary data of *panel B*; **, $p < 0.01$; ***, $p < 0.005$, $n = 4$. *D*, representative images of Shp2 co-stained with PSD95 in cultured neurons with or without cLTP induction ($n = 15$ neurons from 3 cultures for each group). *E*, Pearson's coefficiency of Shp2 with PSD95 in cultured neurons with or without cLTP; ***, $p < 0.005$. *Scale bar*, 20 μm.

$n = 4$), suggesting the Tyr-542 level was also regulated during LTP (Fig. 3, *D* and *E*). We further verified our findings in cultured hippocampal neurons and also found a remarkable increase of the Tyr(P)-542 level at 10 min after cLTP induction without altering the total Shp2 level (Tyr(P)-542 level, 2.51 ± 0.40, $p < 0.01$, cLTP *versus* Ctl, one-way ANOVA, $n = 4$) (Fig. 3, *F* and *G*). Considering that the NMDA receptor plays a critical role in LTP in the hippocampus, we wondered whether the elevation level of Tyr(P)-542 was NMDA receptor dependent. Therefore, we co-incubated APV, which is an antagonist of NMDA receptor, in the neurons during glycine-induced cLTP. Notably, an increase of the level of Tyr(P)-542 was diminished when APV was present during cLTP (1.15 ± 0.10, $p < 0.01$, APV + cLTP *versus* cLTP, one-way ANOVA, $n = 4$), suggesting that the level change of Tyr(P)-542 in cLTP is NMDA receptor dependent (Fig. 3, *F* and *G*).

We had shown that the activity of Shp2 was tightly regulated during LTP. Given that LTP is the cellular mechanism underlying memory, we sought to investigate whether the Tyr(P)-542 level was changed in memory formation *in vivo*. We utilized a well established hippocampus-related memory test, which is contextual fear conditioning. After a training trial containing three times of foot-shocks at 30-s intervals, freezing time within the last 2 min in chambers were recorded and shown to be significantly increased after three foot-shocks (Ctl, 3.39 ± 1.20 s, $n = 4$; CFC 10 min, 92.51 ± 10.78 s, $p < 0.005$, one-way ANOVA, $n = 4$; CFC 60 min, 106.20 ± 11.62 s, $p < 0.001$, one-way ANOVA, $n = 4$) indicating a successful fear learning (Fig. 3*H*). The results showed that the Tyr(P)-542 level was increased at 10 min (1.39 ± 0.054, $p < 0.05$, 10 min *versus* Ctl, one-way ANOVA, $n = 4$) and more remarkably enhanced at 60 min (1.61 ± 0.14, $p < 0.01$, 60 min *versus* Ctl, one-way ANOVA, $n = 4$) after contextual fear conditioning, without affecting the total Shp2 level. As a positive control, both Tyr-1472 (10 min, 2.34 ± 0.14, $p < 0.01$; 60 min, 2.19 ± 0.31, $p < 0.01$, *versus* Ctl, one-way ANOVA, $n = 4$) (19) and Tyr-1070 levels (10 min, 1.66 ± 0.17, $p < 0.01$; 60 min, 1.66 ± 0.11, $p < 0.01$, *versus* Ctl, one-way ANOVA, $n = 4$) (12) of GluN2B were increased in this process, indicating a successful contextual fear conditioning in our paradigm (Fig. 3, *I* and *J*). Taken together, the results from cultured neurons, acute slices, and mice convergently point

FIGURE 1. **Expression profile of Shp2 and phosphorylated Shp2 at Tyr-542.** *A*, Tyr(P)-542 and other related protein levels in different brain regions. Tissue lysates from medial prefrontal cortex (*mPFC*), hippocampus (*Hippo*), thalamus (*Thala*), cerebellum (*Cereb*), amygdala (*Amyg*), pons, and striatum (*Stria*) of adult mice were immunoblotted for Tyr(P)-542 and other associated proteins. A representative blot is shown, the results were from four mice. *B*, summary data of *panel A*. *C*, representative blots for Tyr(P)-542 and other related protein levels in the subcellular fraction of mouse hippocampal lysate. *P2*, crude membrane fraction; *non-PSD*, Triton X-100-soluble fraction; *PSD*, Triton X-100-insoluble fraction. *D*, quantification of *panel C*. The values of Tyr(P)-542 were calculated by Tyr(P)-542 to total Shp2 and normalized to the average of P2 ($n = 4$). *E*, colocalization of endogenous Shp2 (*red*) or Shp2 Tyr(P)-542 (*red*) and PSD-95 (*green*) in cultured hippocampal neurons ($n = 36$ neurons from independent 3 cultures). *Scale bar*, 20 μm. *F*, Pearson's coefficiency of Shp2 or Tyr(P)-542 with PSD95. *G*, three-dimensional iso-surfaced and volume rendered images with various angle views are shown in *I–V*. *H*, colocalization of Shp2 (*green*) with PSD95 (*red*) was assessed by STORM. *Scale bars*, 5 and 1 μm, respectively. *I*, Western blot analysis of Tyr(P)-542 in hippocampus during development ($n = 4$ mice). *J*, summary data of *panel I*. *P*, postnatal day in the figure; all data are displayed as mean ± S.E. unless otherwise stated.

toward to the suggestion that the activity of Shp2 is tightly regulated in LTP and memory formation.

Shp2 Is Critical for Activity-dependent AMPA Receptor Surface Trafficking during LTP—To test whether altered Shp2 enzymatic activity is critical for activity-dependent AMPA receptor surface expression, we used the selective Shp2 inhibitor NSC87877, which binds to the catalytic cleft of the protein-tyrosine phosphatase domain to obliterate phosphatase activity (20). To determine the most effective and specific dose of NSC87877, we applied NSC87877 in HEK293 cells for 30 min

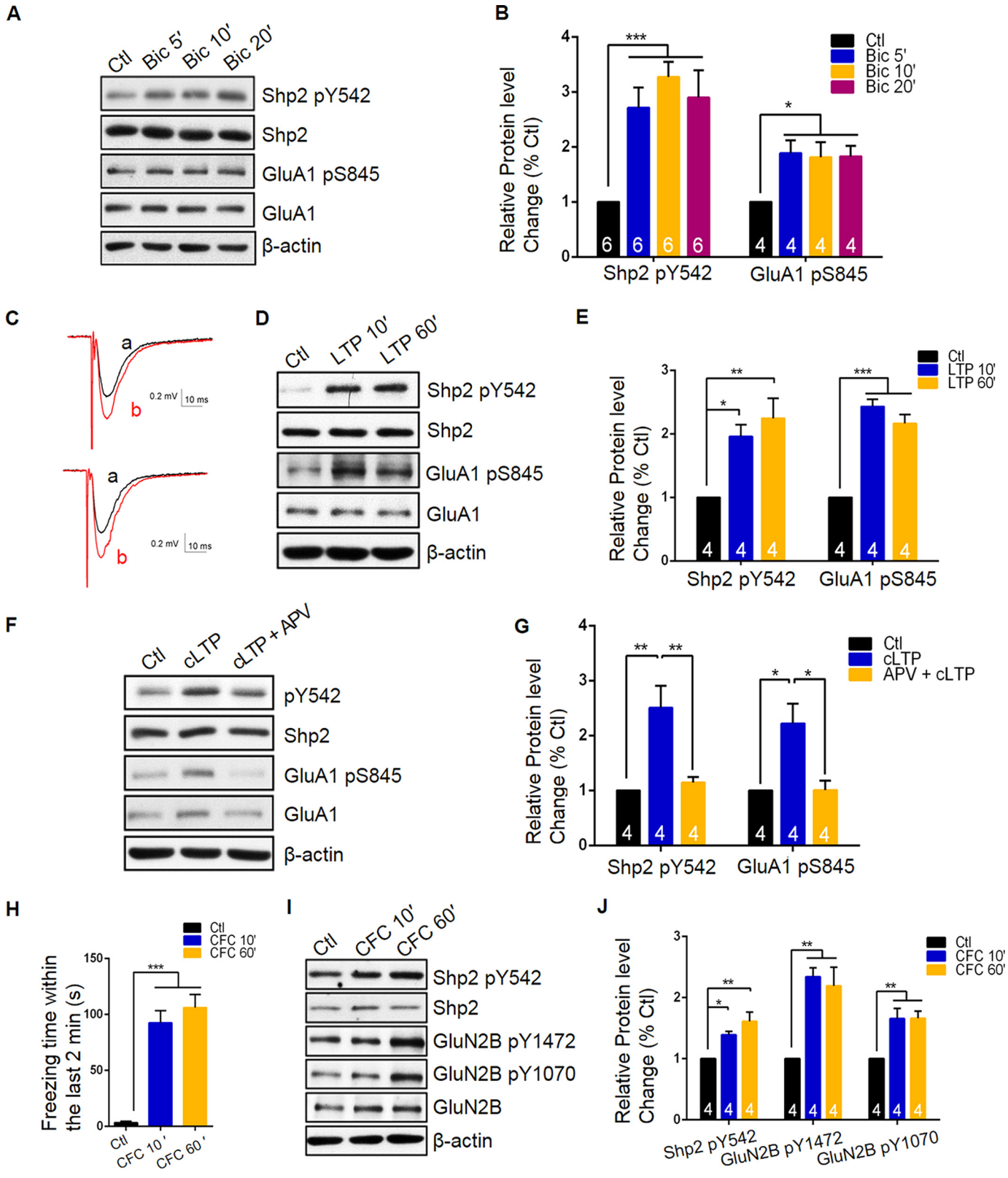

and subsequently the phosphorylation level of Shp2 at Tyr-542 was analyzed by Western blot. The result indicated that 10 μM NSC87877 treatment decreased the Shp2 Tyr(P)-542 level effectively (data not shown). Therefore, we proceeded to apply 10 μM NSC87877 during cLTP induction in cultured hippocampal neurons and found that the inhibitor blocked cLTP inducing the increased Tyr(P)-542 level of Shp2 (cLTP, 2.53 ± 0.18, $p < 0.005$, *versus* Ctl, one-way ANOVA, $n = 4$; NSC87877 + cLTP, 1.25 ± 0.32, $p < 0.01$, *versus* cLTP, one-way ANOVA, $n = 4$; NSC87877, 0.83 ± 0.092, $n = 4$). Previous studies focusing on dysfunctional Shp2 in neurons found that ERK activity was deregulated during neuronal activity and LTP (8–10). Thus, we accessed phosphorylated ERK and total ERK at the same time. The phosphorylation level of ERK (pT202/204) was dramatically decreased in NSC87877 + cLTP treatment compared with cLTP alone (cLTP, 2.00 ± 0.077, $p < 0.005$, *versus* Ctl, one-way ANOVA, $n = 4$; NSC87877 + cLTP, 1.02 ± 0.091, $p < 0.005$, *versus* cLTP, one-way ANOVA, $n = 4$; NSC87877, 0.90 ± 0.10, $n = 4$). Additionally, phosphorylation of GluA1 at Ser-845 was dramatically decreased in NSC87877 + cLTP treatment compared with cLTP alone (cLTP, 1.72 ± 0.15, $p < 0.005$, *versus* Ctl, one-way ANOVA, $n = 4$; NSC87877 + cLTP, 0.85 ± 0.098, $p < 0.005$, *versus* cLTP, one-way ANOVA, $n = 4$; NSC87877, 1.06 ± 0.030, $n = 4$) (Fig. 4, *A* and *B*). These results suggest that Shp2 enzymatic activity is critical for activation of ERK and GluA1 phosphorylation during cLTP. To further characterize the potential role of Shp2 in LTP, hippocampal neurons derived from $Shp2^{flox/flox}$ mice were cultured and infected by adeno-associated virus (AAV)-CaMKII-GFP-Cre to knock out Shp2 in CaMKII-expressing neurons under control of the CaMKII promoter. The neurons infected by AAV-CaMKII-GFP were regarded as a control group in the experiment. On DIV 22, 10 days post-infection, the neuron lysate was subjected to immunoblot analysis. As shown in Fig. 4, *C* and *D*, barely detectable Shp2 (AAV-GFP-cLTP, 1.05 ± 0.046, $p > 0.05$; AAV-Cre-Ctl, 0.51 ± 0.018, $p < 0.005$; AAV-Cre-cLTP, 0.45 ± 0.067, $p < 0.005$, *versus* AAV-GFP-Ctl, one-way ANOVA, $n = 4$), indicating very low expression of Shp2 in the AAV-Cre infected group, was proved a successful AAV-Cre-mediated KO of Shp2 in hippocampal neurons from $Shp2^{flox/flox}$ mice.

We first investigated change of the Ser(P)-845 level after the induction of cLTP in AAV-treated neurons. The Ser(P)-845 level was largely increased after cLTP induction in the AAV-GFP group (AAV-GFP-cLTP, 2.52 ± 0.17, $p < 0.005$, one-way ANOVA, $n = 4$), whereas the Ser(P)-845 level failed to increase after cLTP stimuli in the AAV-Cre group (AAV-Cre-Ctl, 1.02 ± 0.11, $p < 0.005$, one-way ANOVA, $n = 4$; AAV-Cre-cLTP, 1.05 ± 0.077, one-way ANOVA, $p < 0.005$, $n = 4$) (Fig. 4, *C* and *D*), suggesting that Shp2 is required for the increased phosphorylation level of Ser(P)-845 during cLTP. We further evaluated the phosphorylated ERK level after cLTP in AAV-mediated Shp2 KO neurons, finding a elevated level of phosphorylated ERK was blunted in Shp2 KO neurons, which was consistent with our Shp2 inhibitor results (AAV-GFP-cLTP, 2.16 ± 0.29, $p < 0.005$, one-way ANOVA, $n = 4$; AAV-Cre-Ctl, 1.12 ± 0.031, $p < 0.01$, one-way ANOVA, $n = 4$; AAV-Cre-cLTP, 1.05 ± 0.094, one-way ANOVA, $p < 0.01$, $n = 4$).

To confirm the result, surface staining of GluA1 was assessed with and without cLTP induction in the groups. We found a similar result in the AAV-GFP group, showing that surface GluA1 dramatically increased after cLTP induction (without cLTP 1.00 ± 0.027, $n = 15$; with cLTP 1.24 ± 0.037, $n = 19$, one-way ANOVA, $p < 0.005$). However, surface GluA1 in the AAV-Cre group after cLTP was similar to that without cLTP (without cLTP, 0.92 ± 0.050, $n = 16$; with cLTP, 0.87 ± 0.043, $n = 19$, one-way ANOVA, $p < 0.005$) (Fig. 4, *E* and *F*). Collectively, our results suggest Shp2 is required for trafficking of AMPA receptor during cLTP.

We had shown that the activity of ERK increased concomitantly with phosphorylation of Shp2 and GluA1. Given ERK is an important element in surface trafficking of GluA1, we sought to investigate whether ERK was a critical signaling component between Shp2 and GluA1 during cLTP. Thus, we applied a selective MEK inhibitor U0126, which inhibits ERK activity, during cLTP induction in cultured hippocampal neurons and found that the inhibitor blocked cLTP inducing increments of phosphorylated ERK (cLTP, 2.34 ± 0.19, $p < 0.005$, *versus* Ctl, one-way ANOVA, $n = 4$; U0126 + cLTP, 0.37 ± 0.094, $p < 0.005$, *versus* cLTP, one-way ANOVA, $n = 4$; U0126, 0. 42 ± 0.10, $p < 0.005$, *versus* cLTP, one-way ANOVA, $n = 4$) and phosphorylated GluA1 at Ser-845 (cLTP, 1.97 ± 0.037, $p < 0.005$, *versus* Ctl, one-way ANOVA, $n = 4$; U0126 + cLTP, 1.18 ± 0.066, $p < 0.005$, *versus* cLTP, one-way ANOVA, $n = 4$; U0126, 1.05 ± 0.052, $p < 0.005$, *versus* cLTP, one-way ANOVA, $n = 4$). However, cLTP elicited an increased level of Shp2 at Tyr(P)-542, showing that U0126 treatment had a minimal effect on Tyr(P)-542 during cLTP (cLTP, 1.90 ± 0.028, $p < 0.005$, *versus* Ctl, one-way ANOVA, $n = 4$; U0126 + cLTP, 1.84 ± 0.046, $p < 0.005$, *versus* Ctl, one-way ANOVA, $n = 4$; U0126, 1. 08 ± 0.032, $n = 4$). These results suggest that the ERK pathways are downstream of Shp2 activity and play a role in regulating GluA1 phosphorylation during LTP.

Discussion

In this study, we provided evidence that Shp2 was regulated in LTP. We demonstrated that Shp2 was translocated into spines during LTP and was up-regulated, which was represented by a marked increase of the Tyr(P)-542 level. Despite an extensive attempt in earlier studies utilizing genetic approaches

FIGURE 3. **Shp2 Tyr(P)-542 is increased during synaptic activity and contextual fear conditioning.** *A*, represent blots for Tyr(P)-542 and other associated proteins from culture hippocampal neurons treated with 50 μM bicuculline for the indicated times ($n = 6$). *B*, summary data of *panel A*, *, $p < 0.05$; ***, $p < 0.005$, $n = 6$ for Tyr(P)-542, $n = 4$ for Ser(P)-845. *C*, sample traces of 10 (up) or 60 min (down) after LTP induction show average responses during baseline (*a*, *black*) and the last 5 min (*b*, *red*) of the recording. *Scale bar*, 0.2 mV/10 ms. *D*, representative Western blot analysis from a hippocampal slice with or without LTP induction. *E*, summary data of *panel D*, graph represents mean ± S.E.; *, $p < 0.05$; **, $p < 0.01$; ***, $p < 0.005$, $n = 4$. *F*, DIV 18 hippocampal cultures were incubated with or without APV during cLTP induction, representative blots are displayed ($n = 4$). *G*, summary data of *panel F*; *, $p < 0.05$; **, $p < 0.01$, $n = 4$. *H*, freezing time within the last 2 min of contextual fear conditioning were recorded and shown; ***, $p < 0.005$, $n = 4$. *I*, represent blots for Shp2 Tyr(P)-542 and other associated proteins in hippocampus lysate from contextual fear conditioning (*CFC*) in 8–10 week C57BL/6 mice. *J*, quantification of Tyr(P)-542 and associated proteins of *panel I*; *, $p < 0.05$; **, $p < 0.01$, $n = 4$ mice per group.

that lead to fruitful and insightful results, there is limited understanding of the exact Shp2 functional roles in synaptic plasticity and memory. Besides being a signaling node upstream of the MEK-ERK pathway to activate ERK in LTP, Shp2 thereof is also regulated in LTP and memory formation. The data presented show that Shp2 quickly accumulated and responded to LTP stimuli in an acute slice receiving HFS as well as in cultured hippocampal neurons accepting synaptic NMDA receptor activation (Fig. 2). These results, and additional with previous studies, give a more comprehensive understanding of role of Shp2 in long term synaptic plasticity and memory.

Our result demonstrated that Shp2 was uniformly expressed throughout the mice brain, implying numerous and complicated functions of Shp2 in brain. Moreover, we found an appar-

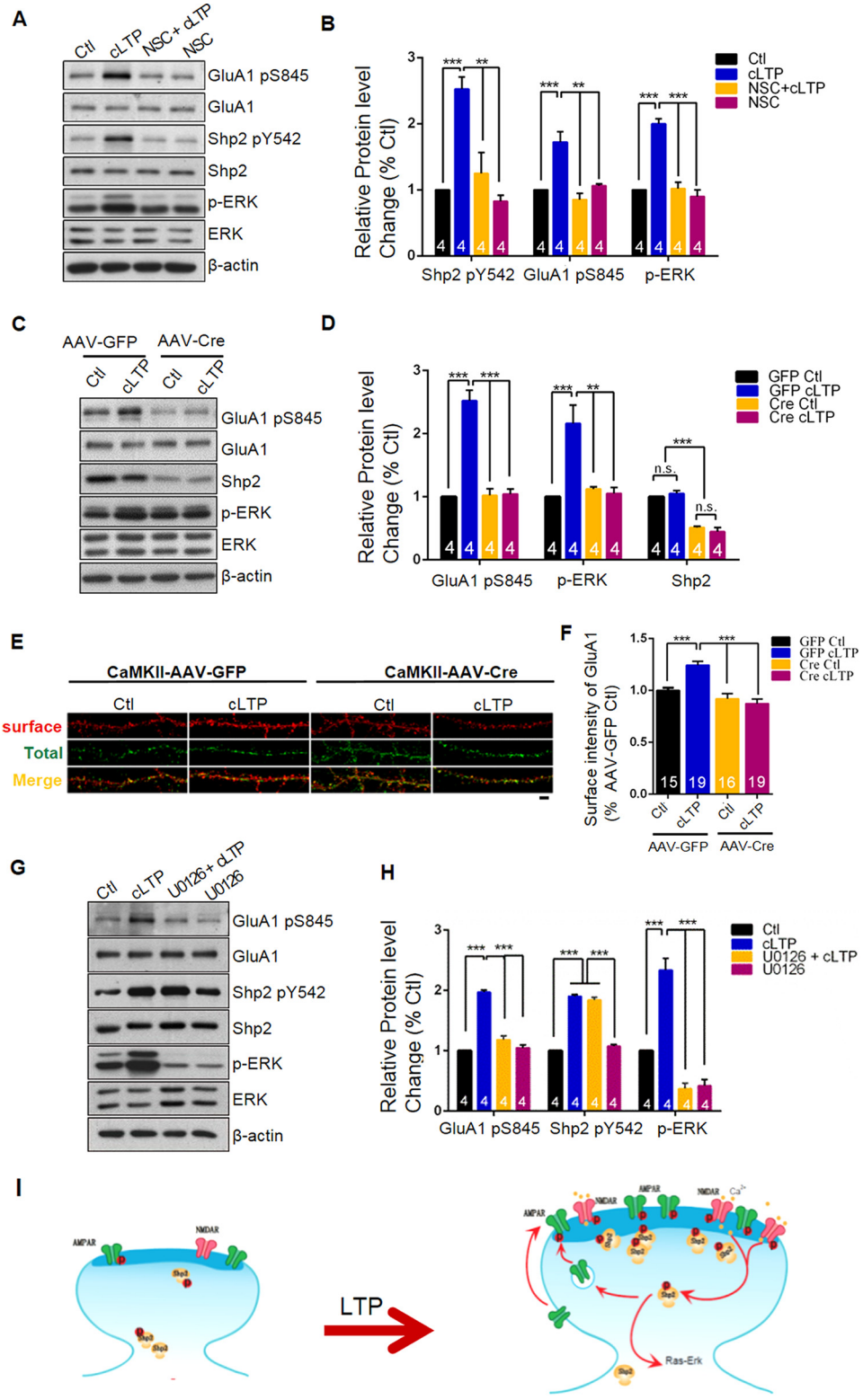

ently higher level of Tyr(P)-542 in pons. Within the pons it is the pneumotaxic center that regulates the change from inhalation to exhalation (21). Thus, we surmised that the activity of Shp2 was possibly related to controlling the respiratory activity by pons.

Previous studies have shown that Shp2 physically associates with two important components of PSD, PSD95 and GluN2B (22–24). In line with those data, we demonstrated that Shp2 was located adjacent to PSD95 in cultured neurons by confocal microscopy and STORM. Notably, the super-resolution microscopy offered a much clearer image of Shp2 colocalization with PSD95 in dendrite spines (Fig. 1). Moreover, during LTP, Shp2 was rapidly translocated into spines, suggesting recruitment of Shp2 into spines serving as some significant functional roles in LTP (Fig. 2). Given Shp2 being physically associated with PSD95 and GluN2B, it will be intriguing to explore whether PSD95 or GluN2B act as a vehicle to mediate the translocation of Shp2 in LTP in the future.

Furthermore, we provided evidence for the first time that the Tyr(P)-452 level of Shp2 was up-regulated in response to cLTP, HFS-induced LTP stimuli, and contextual fear conditioning (Fig. 3). The phosphorylation level of Tyr-542 of Shp2 has been shown to be a concomitant regulation with the activity of Shp2 and at least to some extent, very likely represented the enzymatic activity of Shp2. Thus, we proposed that phosphatase activity of Shp2 was rapidly modulated in LTP and memory formation, rather than being a necessary constituting element required for LTP and memory. Following this suggestion, we showed that the inhibiting activity of Shp2 by its inhibitor NSC87877 resulted in a dampened increase of GluA1 at Ser-845 as well as GluA1 delivery into synapse during cLTP (Fig. 4). Taking advantage of $Shp2^{flox/flox}$ mice, we prepared cultured hippocampal neurons lacking Shp2 via AAV-Cre-mediated KO. The results from Shp2 KO neurons are consistent with other reports (8–10) and our unpublished data,[3] reinforcing the conclusion that Shp2 is critical for AMPA receptor delivery during LTP. Additionally, we found concomitant changes of ERK activity and phosphorylation of GluA1 in cLTP after inhibition of Shp2 activity either by NSC87877 or AAV-mediated KO of Shp2. Activation of ERK signaling facilitates AMPA receptor surface delivery during LTP (25). Furthermore, previous studies indicate that improper Shp2 function results in impaired LTP and memory via deregulated ERK activity (9, 10). Combined using our results and previous studies, ERK has been implicated as a crucial signaling node in the Shp2-related pathway that regulates GluA1 trafficking in LTP.

Heretofore, several potent and specific Shp2 inhibitors, including NSC87877, PHPS1, and GS-493, have been designed and developed for therapeutic treatment targeting deregulated Shp2-related diseases, such as glioblastoma, acute myelogenous leukemia, and gastric cancer (20, 26–29). However, our results indicated that Shp2 was finely regulated and its phosphatase activity was a requisite for AMPA receptor trafficking in LTP. Given a Shp2 inhibitor affecting AMPA receptor surface expression in LTP and thus possibly harming memory, much more caution should be paid to application of the Shp2 inhibitor for treating Shp2-related diseases. In this regard, interruption of Shp2 function by interfering with the association of interacted proteins with Shp2 using peptide-based drugs or impeding upstream/downstream signaling nodes of the Shp2 pathway may be an alternative choice in targeting Shp2-related diseases without afflicting the patients' memory.

Collectively, our results supplemented the illustration of the functional roles of Shp2 in LTP and memory. We not only show that Shp2 is rapidly translocated into spines but also was activated during LTP and contextual fear conditioning. We further revealed that the phosphatase activity of Shp2 was required for AMPA receptor surface expression in LTP by a specific inhibitor of Shp2 and AAV-Cre mediated KO of Shp2 in neurons. Thus, we proposed that it might be cautious when treating patients with Shp2 inhibitors. Last but not least, more comprehensive understanding of Shp2 is vital for our development of therapeutic approaches for Shp2-related diseases.

Experimental Procedures

Hippocampal Neuron Culture and Cell Line—All protocols in our experiments were performed followed Zhejiang University Animal Experimentation Committee guidelines and the guidelines conform to the Guideline for the Care and Use of Laboratory Animals. Efforts were made to minimize the number of animals used and reduce animal suffering. Hippocampal neurons cultures from Sprague-Dawley rats of embryonic day 18 (E18) or newborn (P1–P2) of $Shp2^{flox/flox}$ mice were prepared following the protocol described previously (30) in our laboratory. In general, hippocampal tissue was quickly dissected and then digested in 0.5% trypsin for 15 min at 37 °C. Dissociated neurons were seeded on poly-L-lysine (Sigma)-coated 12-mm coverslips (Deckglaser) at a density of 100,000/dish for immunocytochemistry or 35-mm dish (Corning) at a density of 300,000/dish for biochemical analysis in plating medium (Neurobasal containing 10% horse serum). Four hours later, the plating medium was substituted by culture medium

[3] X. Yan, B. Zhang, W. Lu, L. Peng, Q. Yang, W. Cao, S. Lin, W. Yu, X. Li, Y. Ke, S. Li, W. Yang, and J. Luo, unpublished data.

FIGURE 4. **Inhibition or KO of Shp2 suppresses trafficking of GluA1 to membrane during cLTP.** *A*, hippocampal cultures (DIV 18) were incubated with NSC87877 during cLTP induction. A representative blot is shown. *B*, quantification of *panel A*; *, $p < 0.05$; ***, $p < 0.005$, **, $p < 0.01$, $n = 4$. *C*, cultured hippocampal neurons from $Shp2^{flox/flox}$ mice were infected by AAV-CaMKII-GFP-2A-Cre or AAV-CaMKII-GFP-2A at DIV 8, at DIV 18, cells were treated with glycine for cLTP induction. Protein samples were resolved by SDS-PAGE and blotted for the indicated antibodies. A representative blot is shown. *D*, summary data of *panel C*; **, $p < 0.01$; ***, $p < 0.005$, $n = 4$. *E*, surface GluA1 were labeled with anti-GluA1 antibody and Alexa 546-conjugated anti-mouse secondary antibody (shown in *red*). After permeabilization, total PSD95 was visualized by labeling with anti-PSD95 and Alexa 633-conjugated anti-rabbit secondary antibody (shown in *green*). *Scale bar*, 20 μm. *F*, summary data of *panel E*. The number for AAV-CaMK II-GFP (−/+ cLTP) = 15, 19; the number for (AAV)-CaMK II-GFP-Cre (−/+ cLTP) = 16, 19; ***, $p < 0.005$. *G*, hippocampal cultures (DIV 18) were incubated with 10 μM U0126 during cLTP induction. A representative blot is shown. *H*, quantification of *panel G*; ***, $p < 0.005$, $n = 4$. *I*, summary of our results. After LTP induction, Shp2 was rapidly (time scale of minutes) translocated into spines and the phosphorylation level of Shp2 at Tyr-542 was dramatically enhanced possibly leading to activation of the ERK pathway. This process is critical for the GluA1 subunit of AMPA receptor trafficking to membrane during cLTP.

(Neurobasal media containing 0.5 mM GlutaMax supplemented with 2% B27 and 1% penicillin/streptomycin). Subsequently, half-culture medium was replaced by fresh medium every 4 days. At DIV 4 cells were treated with cytosine arabinoside at a final concentration of 2.5 μM. All cell culture reagents were purchased from GIBCO (Invitrogen) unless stated otherwise.

HEK293 cells were grown in DMEM containing 10% fetal bovine serum plus 1% penicillin/streptomycin. The indicated concentration of NSC87877 was added directly into the culture media for 30 min incubation time before being homogenized.

Western Blotting—Western blotting was performed according to conventional methods with minor modifications (30). Briefly, hippocampal tissue from mice or cultured cells was homogenized in RIPA buffer containing 10 mM Tris, pH 7.4, 150 mM NaCl, 1 mM EDTA, 0.1% SDS, 1% Triton X-100, and 1% sodium deoxycholate (Beyotime) and centrifuged at 16,000 $\times$ *g* for 20 min. Proteins in the supernatant were quantified using a BCA Protein Assay Kit (Thermo), and denatured by boiling in 4$\times$ loading buffer for 5 min. Equal amounts of total protein were loaded onto 10% polyacrylamide-SDS gel and transferred to nitrocellulose membranes (Whatman, GE Healthcare). The membranes were incubated in blocking buffer (2.5% BSA in TBST) for at least 60 min at room temperature, and then incubated with the respective primary antibodies in TBST overnight at 4 °C. After an extensive wash with TBST, the blots were incubated with HRP-conjugated secondary antibody for 1 h in TBST at room temperature. Following washes for 1 h with TBST, immunoreactivity was detected by chemiluminescence with ECL reagent (Bio-Rad). Protein bands were analyzed with Quantity One software (Bio-Rad).

Extraction of Subcellular Fraction—Subcellular fractionation was performed as described (12). Hippocampus from adult mice or the CA1 region of the hippocampal slice was homogenized in cold buffer A (0.32 M sucrose, 10 mM HEPES, pH 7.4) and centrifuged at 1,000 $\times$ *g* for 4 min to remove nuclei and large debris (P1). The supernatant was subsequently centrifuged at 12,000 $\times$ *g* for 20 min to obtain a crude membrane fraction (P2), the pellet was then rinsed twice in buffer B (4 mM HEPES, 1 mM EDTA, pH 7.4) and centrifuged at 12,000 $\times$ *g* for another 20 min, the pellet was further dissolved in buffer C (20 mM HEPES, 100 mM NaCl, 0.5% Trition X-100, pH 7.2). Subsequently, the homogenate was incubated for 15 min and centrifuged at 12,000 $\times$ *g* for 20 min, and this resulting supernatant was considered as the non-postsynaptic density membrane fraction (non-PSD). The pellet was then dissolved in buffer D (20 mM HEPES, 0.15 mM NaCl, 1% Triton X-100, 1% deoxycholic acid, 1% SDS, 1 mM DTT, pH 7.5) for 1 h at 4 °C and subjected to centrifugation at 10,000 $\times$ *g* for 15 min, The supernatant was regarded as the PSD or Triton-insoluble fraction. At last, P2, non-PSD, and PSD were used for Western blot analysis. All buffers were supplemented with protease inhibitors and phosphatase inhibitors.

Induction of Chemical LTP—The cLTP protocol was adopted from previous publications (17, 18). Hippocampal neurons were rinsed twice in non-magnesium ECS (143 mM NaCl, 5 mM KCl, 3 mM $CaCl_2$, 10 mM HEPES, 10 mM glucose, pH 7.4), and incubated in ECS^+ (non-magnesium ECS containing 0.5 μM tetrodotoxin, 1 μM strychnine, 20 μM bicuculline) for 20 min. Afterward, glycine was applied into the ECS^+ for 5 min. After rinsing in non-magnesium ECS twice, neurons were incubated in ECS^+ for the indicated time. In the control group, neurons were treated with ECS^+ throughout the experiment. In the inhibitor group, APV or NSC87877 were applied throughout the process.

Slice Preparation and Field-EPSP Recording—The experiment was carried out as described previously (17). 5–6-Week-old male Sprague-Dawley rats were anesthetized with ether and quickly decapitated. The brain was quickly transferred to ice-cold ACSF (119 mM NaCl, 2.5 mM KCl, 2.5 mM $CaCl_2$, 1.3 mM $MgSO_4$, 1.0 mM NaH_2PO_4, 26.2 mM $NaHCO_3$, 11 mM glucose) saturated with 95% O_2 and 5% CO_2. The hippocampus was carefully separated and 400-μm thick transverse slices were obtained with a vibratome (Leica VT1200S) in ice-cold ACSF and recovered in ACSF at 25 °C for at least 1.5 h before recordings.

The transverse hippocampal slice was then transferred to a submerged recording chamber continuously perfused with ACSF saturated with 95% O_2 and 5% CO_2 at a rate of 4 ml/min. After removing the CA3 area, 100 μM picrotoxin was added in ACSF during recording. Field-EPSPs were recorded in the SC-CA1 region at 0.05 Hz for 30 min of stable baseline recording and 100 Hz/1-s induction stimulation were used to induce LTP and recording was continued for 10 or 60 min. Electrical stimuli were delivered through a bipolar concentric electrode (CBARC75, FHC).

Contextual Fear Conditioning—Before the contextual fear conditioning stimulation, male adult mice (C57BL/6, 8–10 weeks age) were routinely handled for at least 3 days. All fear conditioning stimulations were performed in an NIR Video Fear Conditioning System (Med Associates). After 2 min of freely exploring the chamber, three foot-shocks (2 s duration, 0.6 mA intensity) were delivered at 30-s intervals through the stainless steel rods. After another 2 min habituation in the chambers, mice were transferred to the homecage for 10 or 60 min, then mice were sacrificed for hippocampi collection. The tissue was immediately stored in liquid nitrogen. The chambers were cleaned with 70% ethanol between trials.

Antibodies and Reagents—The primary antibodies used were mouse anti-GluN2B (5530S, Cell Signaling, 1:1,000), rabbit anti-pGluN2B-Y1070 (ab181102, Abcam 1:1,000), rabbit anti-pGluN2B-Y1472 (AB5403, Millipore 1:1,000), rabbit anti-GluN2A (ab133265, Abcam 1:1000), rabbit anti-PSD95 (3409S, Cell Signaling 1:1,000), mouse anti-ERK1/2 (4696S, Cell Signaling 1:2,000), rabbit anti-phospho-ERK1/2 (9101S, Cell Signaling 1:2,000), mouse anti-PSD95 (3409S, Abcam 1:500), rabbit anti-Shp2 (SC-280, Santa Cruz 1:4,000), rabbit anti-pShp2-Y542 (ab62322, Abcam 1:10,000), mouse anti-GluA1 (MAB2263, Millipore 1:3,000), rabbit anti-pGluA1-S845 (04-1073, Millipore 1:3,000), and mouse anti-β-actin (A5316, Sigma 1:10,000). The secondary antibodies were goat anti-rabbit IgG-HRP conjugated and goat anti-mouse IgG-HRP conjugated (31420, 31460, Pierce, 1:10000), donkey anti-mouse Alexa 488 conjugated, donkey anti-rabbit Alexa 546 conjugated, goat anti-rabbit Alexa 633 conjugated (A21206, A11001, A21082, Invitrogen 1:500 for confocal microscopy), STORM-

specific secondary antibodies were donkey anti-rabbit Cy3B (5 μg/ml; generous gift from Hangjun Wu, Facility for Microscopic Imaging Core Facilities, Zhejiang University School of Medicine, Hangzhou China) and donkey anti-mouse Alexa 647 conjugated (712605153, Jackson Laboratory).

Bicuculin (2503), tetrodotoxin (1078), and NSC87877 (2613) were purchased from Tocris. APV (A8054) and NMDA (M3262) were acquired from Sigma, whereas U0126 (number 9903) was acquired from Cell Signaling Technology. AAVs, both AAV-CaMKII-GFP-Cre and AAV-CaMKII-GFP, were packaged by Obio Technology, Shanghai, China.

Immunocytochemistry—We followed the protocol described previously for surface staining of GluA1 (31).

For staining of endogenous Shp2, pShp2 Tyr-542, and PSD95, neurons on coverslips were fixed with 4% paraformaldehyde for 10 min. After a brief rinse in PBS, neurons were then permeabilized and blocked simultaneously in the blocking buffer (0.2% Triton X-100 and 5% BSA in PBS) for 0.5 h. Primary antibodies were then applied in PBS containing 5% BSA overnight at 4 °C. The following day, after three times washing with PBS, secondary antibodies were applied in PBS containing 5% BSA either for 1 h at room temperature or overnight at 4 °C. For staining of GluA1, donkey anti-mouse Alexa 546-conjugated and donkey anti-rabbit Alexa 633-conjugated secondary antibody were used; for colocalization detection between Shp2 and PSD95, donkey anti-mouse Alexa 488-conjugated and donkey anti-rabbit Alexa 546-conjugated secondary antibody were used.

For STORM image, we followed the protocol previously described (29). After fixation, permeability, and blocking, DIV 18 hippocampus neurons were incubated with primary antibody in PBS containing 5% BSA (anti-PSD95, 1:60; anti-Shp2, 1:20) overnight at 4 °C, and washed five times with PBS with each interval of 10 min. After an extensive wash, secondary antibodies were then applied in PBS containing 5% BSA (donkey anti-mouse Alexa 647, 1:50; donkey anti-rabbit Cy3B, 5 μg/ml) overnight at 4 °C. After five times washing in PBS, neurons were further fixed for another 10 min with 4% paraformaldehyde, then the coverslips were kept in PBS for immediate STORM microscopy.

Image Analysis and Quantification—Images were acquired with a confocal microscope (Fluoview FV1000, Olympus). Colocalization ratios of clusters were analyzed using ImageJ with plug-in of JACoP. For surface AMPA receptor intensity, the integrated intensity of individual puncta of the endogenous surface GluA1 on the dendritic protrusions was measured. For Z-stack images of hippocampal neurons, the images were recorded, processed, and analyzed with the help of Imaris software (Imaris software package, Bitplane AG, Zurich, Switzerland) as previously described (32). Acquisition of three-dimensional STORM images was performed using a protocol previously described (33) on a Nikon N-STORM microscope equipped with a ×100 oil immersion objective (CFI Apo ×100 oil NA 1.49 TIRF WD 0.12) and an Andor camera (iXon 897 back illuminated EMCCD). Each image acquisition cycle contained one activation frame (405 nm laser) and five imaging frames (561- or 647-nm lasers). The integration time of the EMCCD was set to 1 frame mode with an EM gain of 30, 5,000–10,000 cycles per channel were taken for the reconstruction of each three-dimensional super-resolution image using Nikon NIS Elements 4.30 software.

Statistical Analysis—All data were analyzed using GraphPad Prism 6 software and represented as mean ± S.E. The comparisons of two groups were compared by Student's *t* test. Data of multiple groups (≥3 groups) were tested using one-way ANOVA followed with Tukey's post hoc test. $p \leq 0.05$ was considered as significant differences.

Author Contributions—B. Z. designed and performed biochemical, immunostaining, and behavior experiments. W. L. designed and performed some biochemical experiments. Y. L. D. and X. Y. Y conducted the electrophysiological experiments. Q. Y. performed neuronal culture and some biochemistry experiments. B. Z., W. L., and W. Y. analyzed the data. B. Z., Y. L. D., W. L., and J. H. L. conceived and coordinated the study and wrote the paper.

Acknowledgments—We thank Professor Yuehai Ke for kindly providing the Shp2$^{flox/flox}$ mice. We are grateful to Hangjun Wu and Sanhua Fang, the Facility for Microscopic Imaging of Zhejiang University School of Medicine, for their assistance in confocal microscopy and super-resolution microscopy.

References

1. Dance, M., Montagner, A., Salles, J. P., Yart, A., and Raynal, P. (2008) The molecular functions of Shp2 in the Ras/mitogen-activated protein kinase (ERK1/2) pathway. *Cell. Signal.* **20,** 453–459
2. Neel, B. G., Gu, H., and Pao, L. (2003) The "Shp"ing news: SH2 domain-containing tyrosine phosphatases in cell signaling. *Trends Biochem. Sci.* **28,** 284–293
3. Araki, T., Nawa, H., and Neel, B. G. (2003) Tyrosyl phosphorylation of Shp2 is required for normal ERK activation in response to some, but not all, growth factors. *J. Biol. Chem.* **278,** 41677–41684
4. Poole, A. W., and Jones, M. L. (2005) A SHPing tale: perspectives on the regulation of SHP-1 and SHP-2 tyrosine phosphatases by the C-terminal tail. *Cell. Signal.* **17,** 1323–1332
5. Prahallad, A., Heynen, G. J., Germano, G., Willems, S. M., Evers, B., Vecchione, L., Gambino, V., Lieftink, C., Beijersbergen, R. L., Di Nicolantonio, F., Bardelli, A., and Bernards, R. (2015) PTPN11 is a central node in intrinsic and acquired resistance to targeted cancer drugs. *Cell Rep.* **12,** 1978–1985
6. Kessels, H. W., and Malinow, R. (2009) Synaptic AMPA receptor plasticity and behavior. *Neuron* **61,** 340–350
7. Malinow, R., and Malenka, R. C. (2002) AMPA receptor trafficking and synaptic plasticity. *Annu. Rev. Neurosci.* **25,** 103–126
8. Kusakari, S., Saitow, F., Ago, Y., Shibasaki, K., Sato-Hashimoto, M., Matsuzaki, Y., Kotani, T., Murata, Y., Hirai, H., Matsuda, T., Suzuki, H., Matozaki, T., and Ohnishi, H. (2015) Shp2 in forebrain neurons regulates synaptic plasticity, locomotion, and memory formation in mice. *Mol. Cell Biol.* **35,** 1557–1572
9. Lee, Y. S., Ehninger, D., Zhou, M., Oh, J. Y., Kang, M., Kwak, C., Ryu, H. H., Butz, D., Araki, T., Cai, Y., Balaji, J., Sano, Y., Nam, C. I., Kim, H. K., Kaang, B. K., *et al.* (2014) Mechanism and treatment for learning and memory deficits in mouse models of Noonan syndrome. *Nat. Neurosci.* **17,** 1736–1743
10. Pagani, M. R., Oishi, K., Gelb, B. D., and Zhong, Y. (2009) The phosphatase SHP2 regulates the spacing effect for long-term memory induction. *Cell* **139,** 186–198
11. Suzuki, T., Matozaki, T., Mizoguchi, A., and Kasuga, M. (1995) Localization and subcellular distribution of SH-PTP2, a protein-tyrosine phosphatase with Src homology-2 domains, in rat brain. *Biochem. Biophys. Res. Commun.* **211,** 950–959
12. Lu, W., Fang, W., Li, J., Zhang, B., Yang, Q., Yan, X., Peng, L., Ai, H., Wang,

J. J., Liu, X., Luo, J., and Yang, W. (2015) Phosphorylation of tyrosine 1070 at the GluN2B subunit is regulated by synaptic activity and critical for surface expression of *N*-methyl-D-aspartate (NMDA) receptors. *J. Biol. Chem.* **290,** 22945–22954
13. Gauthier, A. S., Furstoss, O., Araki, T., Chan, R., Neel, B. G, Kaplan, D. R., and Miller, F. D. (2007) Control of CNS cell fate decisions by SHP-2 and its dysregulation in Noonan syndrome. *Neuron* **54,** 245–262
14. Sanz-Clemente, A., Matta, J. A., Isaac, J. T., and Roche, K. W. (2010) Casein kinase 2 regulates the NR2 subunit composition of synaptic NMDA receptors. *Neuron* **67,** 984–996
15. Corera, A. T., Doucet, G., and Fon, E. A. (2009) Long-term potentiation in isolated dendritic spines. *PLoS ONE* **4,** e6021
16. Tang, Y., Ye, M., Du, Y., Qiu, X., Lv, X., Yang, W., and Luo, J. (2015) EGFR signaling upregulates surface expression of the GluN2B-containing NMDA receptor and contributes to long-term potentiation in the hippocampus. *Neuroscience* **304,** 109–121
17. Zhang, X. M., Yan, X. Y., Zhang, B., Yang, Q., Ye, M., Cao, W., Qiang, W. B., Zhu, L. J., Du, Y. L., Xu, X. X., Wang, J. S., Xu, F., Lu, W., Qiu, S., Yang, W., and Luo, J. H. (2015) Activity-induced synaptic delivery of the GluN2A-containing NMDA receptor is dependent on endoplasmic reticulum chaperone Bip and involved in fear memory. *Cell Res.* **25,** 818–836
18. Lu, W., Man, H., Ju, W., Trimble, W. S., MacDonald, J. F., and Wang, Y. T. (2001) Activation of synaptic NMDA receptors induces membrane insertion of new AMPA receptors and LTP in cultured hippocampal neurons. *Neuron* **29,** 243–254
19. Barki-Harrington, L., Elkobi, A., Tzabary, T., and Rosenblum, K. (2009) Tyrosine phosphorylation of the 2B subunit of the NMDA receptor is necessary for taste memory formation. *J. Neurosci.* **29,** 9219–9226
20. Chen, L., Sung, S. S., Yip, M. L., Lawrence, H. R., Ren, Y., Guida, W. C., Sebti, S. M., Lawrence, N. J., and Wu, J. (2006) Discovery of a novel shp2 protein tyrosine phosphatase inhibitor. *Mol. Pharmacol.* **70,** 562–570
21. Saladin, K. S. (2007) *Anatomy and Physiology the Unity of Form and Function*, McGraw-Hill, Dubuque, IA
22. Peng, H. Y., Chen, G. D., Lai, C. Y., Hsieh, M. C., and Lin, T. B. (2012) Spinal SIRPα1-SHP2 interaction regulates spinal nerve ligation-induced neuropathic pain via PSD-95-dependent NR2B activation in rats. *Pain* **153,** 1042–1053
23. Husi, H., Ward, M. A., Choudhary, J. S., and Blackstock, W. P., and Grant, S. G. (2000) Proteomic analysis of NMDA receptor-adhesion protein signaling complexes. *Nat. Neurosci.* **3,** 661–669
24. Lin, S. Y., Wu, K., Len, G. W., Xu, J. L., Levine, E. S., Suen, P. C., Mount, H. T., and Black, I. B. (1999) Brain-derived neurotrophic factor enhances association of protein tyrosine phosphatase PTP1D with the NMDA receptor subunit NR2B in the cortical postsynaptic density. *Mol. Brain Res.* **70,** 18–25
25. Zhu, J. J., Qin, Y., Zhao, M., Van Aelst, L., and Malinow, R. (2002) Ras and Rap control AMPA receptor trafficking during synaptic plasticity. *Cell* **110,** 443–455
26. Grosskopf, S., Eckert, C., Arkona, C., Radetzki, S., Böhm, K., Heinemann, U., Wolber, G., von Kries, J. P., Birchmeier, W., and Rademann, J. (2015) Selective inhibitors of the protein tyrosine phosphatase SHP2 block cellular motility and growth of cancer cells *in vitro* and *in vivo*. *ChemMedChem* **10,** 815–826
27. Hellmuth, K., Grosskopf, S., Lum, C. T., Würtele, M., Röder, N., von Kries, J. P., Rosario, M., Rademann, J., and Birchmeier, W. (2008) Specific inhibitors of the protein tyrosine phosphatase Shp2 identified by high-throughput docking. *Proc. Natl. Acad. Sci. U.S.A.* **105,** 7275–7280
28. Bentires-Alj, M., Paez, J. G., David, F. S., Keilhack, H., Halmos, B., Naoki, K., Maris, J. M., Richardson, A., Bardelli, A., Sugarbaker, D. J., Richards, W. G., Du, J., Girard, L., Minna, J. D., Loh, M. L., *et al.* (2004) Activating mutations of the noonan syndrome-associated *SHP2*/*PTPN11* gene in human solid tumors and adult acute myelogenous leukemia. *Cancer Res.* **64,** 8816–8820
29. Chan, G., Kalaitzidis, D., and Neel, B. G. (2008) The tyrosine phosphatase Shp2 (PTPN11) in cancer. *Cancer Metastasis Rev.* **27,** 179–192
30. Lu, W., Ai, H., Peng, L., Wang, J. J., Zhang, B., Liu, X., and Luo, J. H. (2015) A novel phosphorylation site of *N*-methyl-D-aspartate receptor GluN2B at S1284 is regulated by Cdk5 in neuronal ischemia. *Exp. Neurol.* **271,** 251–258
31. Diering, G. H., Gustina, A. S., and Huganir, R. L. (2014) PKA-GluA1 coupling via AKAP5 controls AMPA receptor phosphorylation and cell-surface targeting during bidirectional homeostatic plasticity. *Neuron* **84,** 790–805
32. Shen, H., Sesack, S. R., Toda, S., and Kalivas, P. W. (2008) Automated quantification of dendritic spine density and spine head diameter in medium spiny neurons of the nucleus accumbens. *Brain Struct. Funct.* **213,** 149–157
33. Bates, M., Jones, S. A., and Zhuang, X. (2013) Stochastic optical reconstruction microscopy (STORM): a method for superresolution fluorescence imaging. *Cold Spring Harb. Protoc.* **2013,** 498–520